Janus single layers of In_2SSe: A first-principles study

A. Kandemir[1,*] and H. Sahin[2,3,†]

[1]*Department of Materials Science and Engineering, Izmir Institute of Technology, 35430 Izmir, Turkey*

[2]*Department of Photonics, Izmir Institute of Technology, 35430 Izmir, Turkey*

[3]*ICTP-ECAR Eurasian Center for Advanced Research, Izmir Institute of Technology, 35430 Izmir, Turkey*

(Received 6 January 2018; revised manuscript received 20 March 2018; published 11 April 2018)

By performing first-principles calculations, we propose a stable direct band gap semiconductor Janus single-layer structure, In_2SSe. The binary analogs of the Janus structure, InS and InSe single layers are reviewed to evince the structural and electronic relation with In_2SSe. The structural optimization calculations reveal that a Janus In_2SSe single layer has hexagonal geometry like the InS and InSe single layers, which are also its structural analogs. The Janus single layer is dynamically stable, as indicated by the phonon spectrum. The electronic band diagram of the Janus structure shows that an In_2SSe single layer is a direct band gap semiconductor, in contrast to its analogs, InS and InSe single layers, which are indirect band gap semiconductors. Nevertheless, it is found that the strain effect on electronic properties of the InS and InSe single layers designates the electronic structure of the Janus single layer. A rough model for the construction of the electronic band diagram of the Janus structures is discussed, and it is indicated that the difference in work functions of chalcogenide sides in the Janus structure determines the construction of the electronic structure. It is found that the Janus structure is a robust direct gap semiconductor under tolerable strain; for that reason, the Janus In_2SSe single layer is a candidate for optoelectronic nanodevice applications.

DOI: 10.1103/PhysRevB.97.155410

I. INTRODUCTION

Two-dimensional (2D) materials have received extensive attention after the discovery of graphene's highly conductive stable ultrathin structure [1,2]. Following graphene, transition-metal dichalcogenides (TMDs) have triggered huge interest and have become another famous family of 2D materials thanks to their extraordinary electronic and device properties [3–9]. By virtue of rapid growth and demand for new 2D materials, both experimental and theoretical studies have been focusing on post-2D materials in recent years [10–18].

As a member of the group-III-V binary compounds, InSe has received interest due to its widely broad optical response and electronic properties [19]. In recent years, thin-film InSe and few-layer InSe have been studied to explore their outstanding electronic properties and produce nanodevices as photodetectors and a field emission transistor with other two-dimensional materials, especially with graphene [20,21]. A broad band gap range has been shown by quantum confinement effects of exfoliated InSe nanosheets [22]. Moreover, the direct-to-indirect crossover of two-dimensional InSe crystals was demonstrated by Mudd *et al.* [23]. Recently, Bandurin *et al.* successfully synthesized s single layer of InSe that is stabilized with *h*-BN encapsulation [24]. Afterwards, a limitation in the fabrication of 2D InSe was overcome by Yang *et al.* [20] with the achievement of wafer-scale synthesis. In addition, lattice thermal conductivity of 2D InSe was studied and calculated to be 27.6 W mK^{-1}, and this value was reduced more with decreasing the flake size of InSe crystals [25]. It was shown that the optical contrast was modified by using bandpass filters, and optimization of the optical contrast of 2D InSe can be achieved in transparent substrates [26]. Furthermore, it was also found that the other indium chalcogenide, InS, has a wide-ranging optical response and also preserves highly anisotropic electrical resistivity [27]. InS crystals have an orthorhombic structure; however, it was demonstrated that the 2D version of InS exists in the hexagonal geometry as an InSe single-layer structure [28]. Therefore, InS and InSe single layers can be used together to widen the area of optoelectronic 2D materials for next generation due to their tunable and optimized functionalities for electronic and optoelectronic applications.

More recently, a different method was achieved for tailoring 2D materials designed at the atomic level: the formation of Janus crystals. Like in computational studies [29,30], the experimental work of Lu *et al.* [31] modified the MoS_2 structure as S-Mo-Se sandwiched layers, and later, the experimental study of Zhang *et al.* [32] switched the Se atomic layer of $MoSe_2$ with S atoms and produced the Janus MoSSe single layer. Additionally, a critical change in dynamical and electronic properties in the Janus structure was shown in their studies. By experimental realization of the Janus MoSSe structure [31,32], covalently bonded layers of other 2D chalcogenides or post-2D materials can be tailored to expose novelties. With this goal, InS and InSe single layers may lead to novel findings due to their extraordinary electronic and optic properties. Therefore, the single-layer Janus structure In_2SSe, from an InS or InSe single layer, is worth investigating.

In this paper, we present the stable 2D Janus material In_2SSe with the structural, vibrational, and electronic properties of

*alikandemir@iyte.edu.tr

†hasansahin@iyte.edu.tr

the Janus structure. Even though the Janus structure keeps the structural properties of the binary analogs, InS and InSe single layers, the In_2SSe single layer exhibits different electronic properties. Moreover, a model is discussed to explain the reason for the change in electronic properties and the construction of the electronic band diagram of a Janus structure. The rest of the paper is organized as follows: computational methodology is given in Sec. II. The structural, electronic, and vibrational properties of single-layer In_2SSe are presented in Sec. III. The strain dependence properties of the In_2SSe single layer are shown in Sec. IV. Section V is devoted to the conclusion of our results.

II. COMPUTATIONAL METHODOLOGY

By using the plane-wave basis projector-augmented wave (PAW) method as implemented in the Vienna Ab initio Simulation Package (VASP) [33,34], first-principles calculations are performed to investigate the Janus In_2SSe single layer. For the exchange-correlation part of the calculations, the generalized gradient approximation (GGA) in the Perdew-Burke-Ernzerhof (PBE) form, which has been well established to describe indium chalcogenides, was employed [35]. The van der Waals (vdW) correction to the GGA functional is included by using the density functional theory long-range dispersion correction (DFT-D2) method of Grimme [36]. The underestimation of the band gap given by pure GGA within the inclusion of spin-orbit coupling (SOC) is corrected by applying the Heyd-Scuseria-Ernzerhof (HSE) screened-nonlocal-exchange functional of the generalized Kohn-Sham scheme [37].

While performing all calculations, a plane-wave basis set with a kinetic-energy cutoff of 400 eV is used. For the convergence criterion, the total-energy difference between the sequential steps in the calculations is taken to be 10^{-5} eV. The total force in the unit cell is reduced to a value of less than 10^{-4} eV/Å. To hinder interactions between the adjacent cells, at least 13-Å vacuum spacing is used along the z direction. All calculations are performed with the spin-polarized case when considering spin-orbit interactions. The analysis of the charge transfers in the structures is determined with the Bader technique [38]. The vibrational properties are obtained with the PHONOPY code [39], which uses the force constants calculated with the finite-displacement method.

III. STRUCTURAL, VIBRATIONAL, AND ELECTRONIC PROPERTIES OF THE JANUS In_2SSe SINGLE LAYER

Figure 1(a) shows the geometric structure of the Janus In_2SSe single layer. As seen in Fig. 1(a), the Janus structure preserves the symmetry and structure of single layers of its binary analogs, which are InS and InSe. For a complete discussion on the Janus single layer of In_2SSe, it is essential to review single layers of InS and InSe.

InS and InSe single layers consist of covalently bonded surface chalcogenides with two layers of In ions in the shell of the structure. The crystal structures of InS and InSe have a hexagonal lattice, and their calculated lattice parameters, $a = b$, are found to be 3.81 and 3.95 Å, respectively. For InS and InSe single layers, the distances between In atoms in the middle layers are found to be 2.79 and 2.78 Å, respectively.

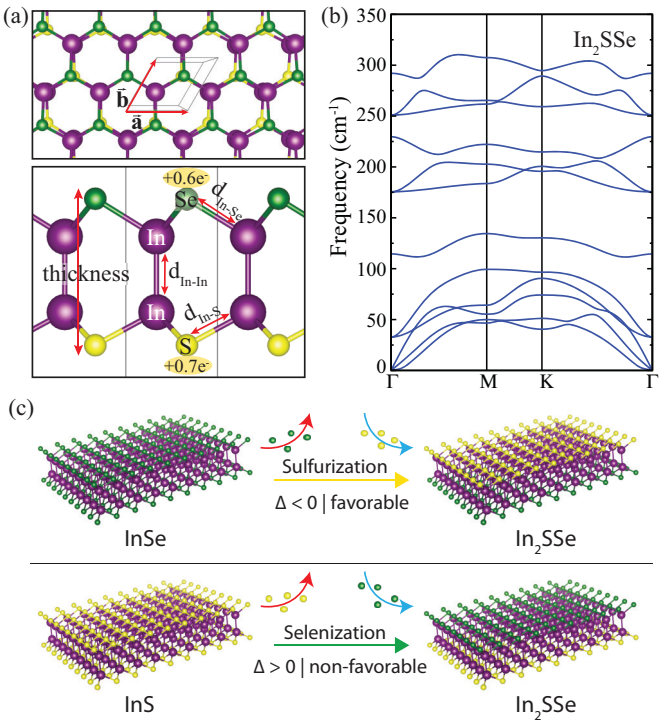

FIG. 1. (a) Top (perspective) and side views of the geometric structure of the Janus In_2SSe single layer. Purple, yellow, and green balls show In, S, and Se atoms, respectively. (b) Phonon band diagram of the Janus In_2SSe single layer. (c) Pathway to synthesizing the Janus structure. Δ indicates the total-energy difference between the final energy (Janus In_2SSe) and initial energy (InSe/InS) of single-layer structures.

The distances between In-S and In-Se are found to be 2.53 and 2.65 Å, respectively. The difference between the uppermost and lowermost atomic layers of a 2D material along the c-axis direction was determined as the thickness of a 2D structure. The thicknesses of InS and InSe single layers are calculated to be 5.30 and 5.49 Å, respectively. In total-energy calculations, we find that both single-layer crystals have a nonmagnetic ground state. Bader charge analyses showed that S atoms receive 0.7 e^- from In atoms and Se atoms receive 0.6 e^- from In atoms. Cohesive energies of InS and InSe single layers are calculated to be 3.58 and 3.33 eV/atom, respectively. Thus, formation of the sulfide form of indium chalcogenides is more favorable than the selenide form.

The Janus In_2SSe single layer consists of covalently bonded surface layers, one side S and one side Se, with two layers of In ions in the shell. The structure of Janus In_2SSe has a hexagonal unit cell with lattice parameters $a = b$, which are calculated to be 3.88 Å. The bond lengths of In-In, In-S, and In-Se are found to be 2.78, 2.55, and 2.64 Å, respectively. Apparently, interaction of In atoms remains unchanged in the Janus structure, whereas the first effect on the structural parameters is found in the interaction between the chalcogenides and In atoms. It is seen that the sulfide side experiences tensile strain, and the selenide side experiences compressive strain. The thickness of the Janus In_2SSe structure is calculated to be 5.39 Å, which is the average value of binary analog single layers' thicknesses. The ground state of the Janus In_2SSe is

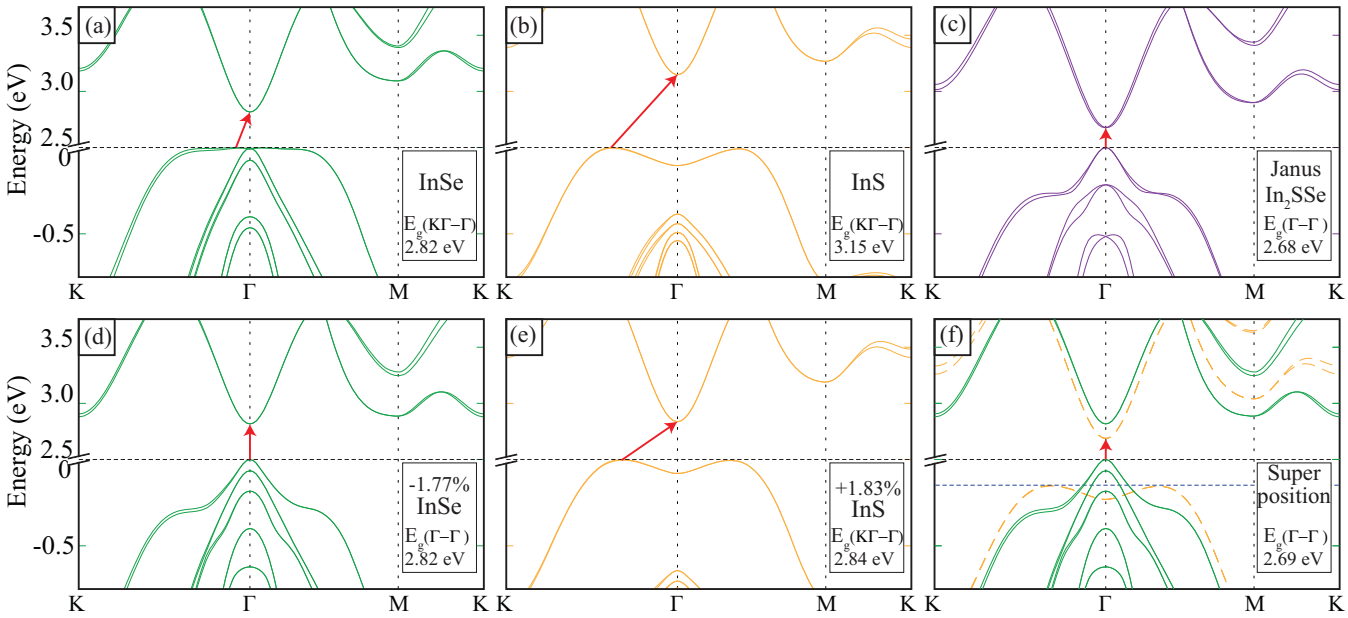

FIG. 2. The electronic band structure of (a) InSe, (b) InS single layers, and (c) Janus In_2SSe. The electronic band structure of strained (d) InSe and (e) InS single layers. The Fermi level is set to zero, and for better projection, an energy range between 0 and 2.5 eV is scissored in the y axis. (f) The electronic band structures' superposition of strained InS and InSe; however, the Fermi level of InS is shifted due to the vacuum level.

found to be in the nonmagnetic state. Moreover, Bader charge analysis of the Janus structure shows a negligible difference compared to InS and InSe single layers. Besides its covalent character, strong ionic character is seen in the Janus structure, like in InS and InSe single layers.

The phonon dispersion diagram for the Janus In_2SSe structure is shown in Fig. 1(b). There are two indium, one sulfur, and one selenium atoms, for a total of four atoms within the primitive unit cell of the Janus structure; therefore, its phonon spectrum includes 12 phonon branches, 3 acoustic and 9 optical. Based on basal plane symmetry of two-dimensional materials, nine optical phonon branches consist of three singly degenerate (115, 230, and 292 cm^{-1}) and three doubly degenerate (33, 176, and 251 cm^{-1}) vibrational modes. As seen from Fig. 1(b), all phonon modes with positive eigenfrequencies in the Brillouin zone indicate that the Janus In_2SSe single layer is dynamically stable; thus, it is shown that synthesis of the Janus structure is possible as a freestanding single layer.

In addition, the cohesive energy of the Janus In_2SSe single layer is found to be 3.50 eV/atom, which is between the values of the binary analogs. This high cohesive energy means that intramolecular bonds in the In_2SSe single layer have strong bond energy. To examine the experimental realization of the Janus In_2SSe single layer, we also check the sulfurization and selenization. It was found that transformation from InSe to In_2SSe is favorable and shows exothermic formation energy, whereas InS to In_2SSe is not favorable and requires energy to form the In_2SSe Janus structure. The outcome from total-energy calculations is schematically illustrated in Fig. 1(c). Sulfurization of a 2D metal selenide is found to be an easy route to achieve the Janus metal chalcogenide single layer, as demonstrated in work of Zhang *et al.* [32], which synthesizes the Janus MoSSe single layer via sulfurization of the $MoSe_2$ single layer.

The electronic properties of InSe and InS single layers were investigated and are shown in Figs. 2(a) and 2(b), respectively. These single layers are similar indirect band gap semiconductors, and their valence-band maximum (VBM) and conduction-band minimum (CBM) points reside at the K-Γ (close to the Γ point) and Γ points, respectively. Apart from band dispersions, the main difference seems to be in the values of the band gap, which are 3.15 and 2.82 eV for InS and InSe single layers, respectively. The calculated electronic band structure of the Janus In_2SSe single layer are shown in Fig. 2(c).

It is found that the Janus structure of In_2SSe is a direct band gap semiconductor with its VBM and CBM residing at the Γ symmetry point. The energy band gap of the Janus structure calculated within GGA+SOC+HSE06 is found to be 2.68 eV, which corresponds to the blue color in visible light. Similarly, the Janus MoSSe single layer was also calculated and measured to be a direct band gap semiconductor with an ∼1 eV lower band gap compared to the Janus In_2SSe single layer [32]. In addition, work-function values of InS, InSe, and the S side and Se side of In_2SSe single layers are calculated to be 6.34, 5.93, 6.00, and 5.86 eV, respectively. Obviously, work-function values decrease on both sides of the Janus structure compared to its binary analogs. All of the structural and electronic properties of InS and InSe single layers are summarized in Table I to easily compare them with the properties of the Janus In_2SSe single layer.

Although the binary analogs are indirect semiconductors, direct band gap behavior occurs in the electronic structure of the ternary Janus In_2SSe single layer. The reason for this behavior is found to be tensile and compressive strains on the binary analogs of the Janus structure, as mentioned before. Then, strain values as a percentage are calculated from lattice constants of the InS and InSe single layer while the

TABLE I. The calculated ground-state properties of the Janus In_2SSe single-layer structure: lattice parameters of the primitive unit cell a and b; the distance between In atoms d_{In-In}; the distance between In and S/Se atoms $d_{In-S/Se}$; the thickness of a single layer t; the magnetic state; the total amount of charge received by the S and Se atoms, $\Delta\rho_S$ and $\Delta\rho_{Se}$, respectively; the cohesive energy per atom in the unit cell E_{coh}; the energy band gap of the structure calculated within GGA+SOC+HSE06 E_g; and the work function for In_2SSe, which is determined as the S side and Se side, Φ_S and Φ_{Se}, respectively. NM denotes nonmagnetic.

	a (Å)	b (Å)	d_{In-In} (Å)	d_{In-S} (Å)	d_{In-Se} (Å)	t (Å)	Magnetic state	$\Delta\rho_S$ (e)	$\Delta\rho_{Se}$ (e)	E_{coh} (eV/atom)	E_g (eV)	Φ_S (eV)	Φ_{Se} (eV)
InS	3.81	3.81	2.79	2.53		5.30	NM	0.7		3.58	3.15	6.34	
InSe	3.95	3.95	2.78		2.65	5.49	NM		0.6	3.33	2.82		5.93
In_2SSe	3.88	3.88	2.78	2.55	2.64	5.39	NM	0.7	0.6	3.50	2.68	6.00	5.86

lattice constant of the Janus structure is used as a reference. Upon the formation of the Janus structure, the sulfide side is exposed to 1.83% tensile strain, whereas the selenide side is exposed to 1.77% compressive strain. Therefore, strained InS and InSe single-layer structures are investigated to clarify the direct band gap behavior of the In_2SSe single layer. The compressively strained InSe single layer's electronic band diagram is obtained, and direct band gap behavior is seen. In other words, a clean VBM residing at the Γ point is achieved [Fig. 2(d)]. On the other hand, a clean CBM residing at the Γ point and a single degenerate band are observed in the electronic band diagram of a tensile-strained InS single layer [Fig. 2(e)].

For heterostructures of two materials, especially for semiconductors, construction of the electronic band diagram at the heterojunction is done via the electronic affinity rule, also called Anderson's rule, which expresses that vacuum level energies of the materials are at the same energy level. Therefore, the band alignment of the materials is shaped with the fusing of Fermi levels at the junction due to equilibrium conditions. We find that the binary analogs of the Janus materials generate (or form) the electronic band diagram of the Janus structures through the adjustment of the Fermi levels of the electronic band diagrams of the strained analogs while considering Anderson's rule, which states that each Janus half has to have the same vacuum energy level. Therefore, if the electronic band diagrams of the strained analog structures are shifted due to their work-function values in the In_2SSe single layer, which indicate the Fermi level (or VBM in the figures) of the Janus single layer, a resemblance to the Janus structure's electronic band diagram can be achieved, as illustrated in Fig. 2(f). By filling of the correct energy bands with electrons, the superposition illustration shown in Fig. 2(f) should generate the electronic band diagram of the In_2SSe single layer in the end. We believe that the uniformness of the electronic band diagram and energy band gap value that is achieved with this method should not be an exception. A slight inconsistency between the electronic band diagrams is related to the polarity in the Janus single layer, which causes an electric-field effect on the electronic structure, as seen in Fig. 2(c) around the Γ

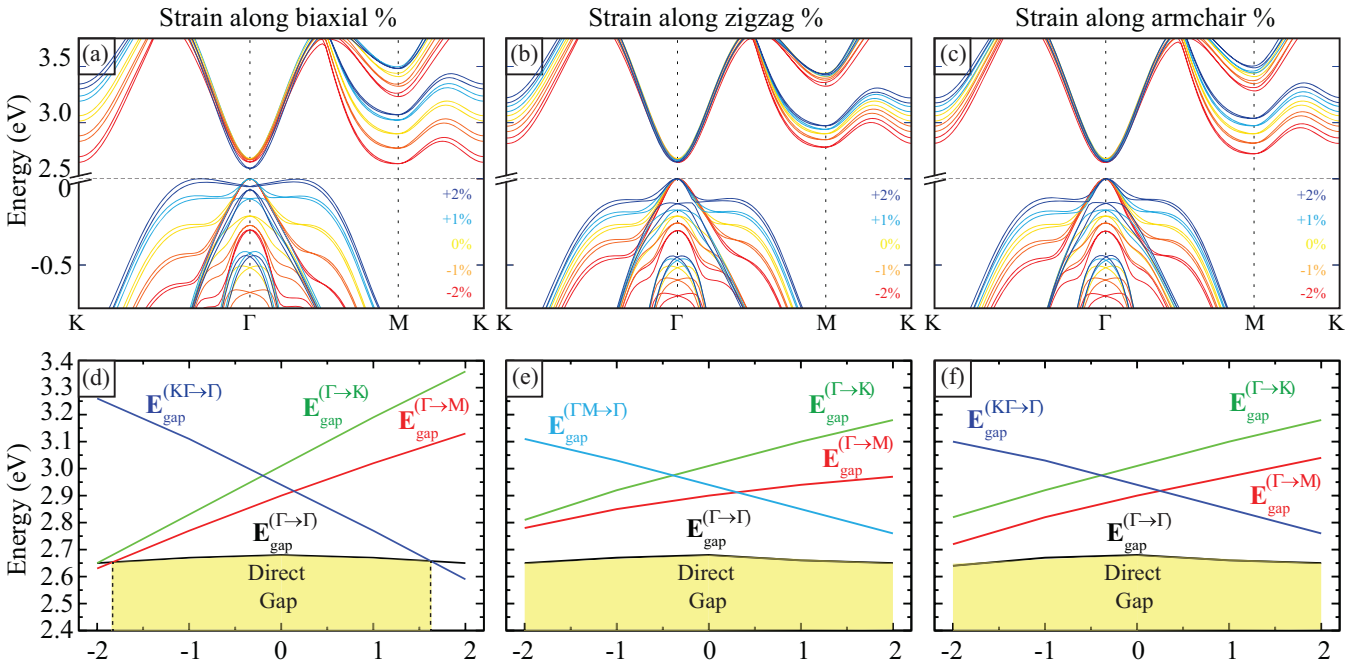

FIG. 3. Strain-dependent electronic band diagram of the Janus In_2SSe structure along the (a) biaxial, (b) zigzag, and (c) armchair directions. The Fermi level is set to zero, and for better projection, an energy range between 0 and 2.5 eV is scissored in the y axis. Strain-dependent band gap crossovers along the (d) biaxial (e) zigzag (f) armchair directions.

point. Apparently, the mixture of the tensile and compressively strained sulfide and selenide sides is the origin of the Janus structure's direct band gap nature.

IV. STRAIN-DEPENDENT ELECTRONIC PROPERTIES OF THE JANUS STRUCTURE

The electronic configuration of materials defines not only atomic coordination but also their electronic and vibrational properties. Accordingly, characteristic properties of materials are strongly dependent on the strain effects. In addition, the effects caused by strain in ultrathin materials appear to be drastic. Therefore, it is essential to consider strain effects on the electronic properties of ultrathin materials.

Here, we demonstrate three main strain mechanisms in 2D materials and reveal the strain effect on the electronic properties of the Janus In_2SSe single layer. Biaxial and planar uniaxial strains (tensile and compressive) are applied to the Janus structure, and changes in the band gap properties are investigated. Figure 3 shows a strain-dependent electronic band diagram of the Janus In_2SSe structure and strain-dependent band gap crossovers. Overall, the direct band character of the Janus structure shows a strain-independent, robust direct band gap between 2.63 and 2.68 eV, especially for planar uniaxial strains. Additionally, even in biaxial strain, the Janus structure is a robust direct semiconductor between 1.8% compressive strain and 1.6% tensile strain.

For strain-dependent electronic band diagrams, it can be generalized that there are three different trends, which are the Γ to M indirect gap for compressive strain values, the Γ to Γ direct gap in the tolerable strain region between the compressive and tensile strain ranges, and the K-Γ or M-Γ to Γ indirect gap for tensile strain values. If we consider the trends' rate of change, the $\Gamma \rightarrow \Gamma$ gap is nearly constant for all types of strain. The gap of the $K\Gamma \rightarrow \Gamma$ transition (for strain in the biaxial and armchair directions) and that of the $M\Gamma \rightarrow \Gamma$ transition (for strain in the zigzag direction) dramatically increase under shrinking and decrease under stretching; for high tensile-strain values, the gap forges ahead in this way, making the Janus structure an indirect semiconductor. In contrast, the gaps of the $\Gamma \rightarrow M$ and $\Gamma \rightarrow K$ transitions drastically decrease under shrinking and are altered under stretching. The rates of change of the $\Gamma \rightarrow M$ and $\Gamma \rightarrow K$ transitions are nearly the same under strain along the armchair direction, and for higher compressive-strain values, the indirect band gap of the $\Gamma \rightarrow M$ transition becomes dominant in the Janus structure. However, the rate of change of the $\Gamma \rightarrow K$ transition is higher than the rate of change of the $\Gamma \rightarrow M$ transition, thus; for higher compressive-strain values in the zigzag direction, the indirect band gap of the $\Gamma \rightarrow M$ transition becomes dominant in the Janus structure. Due to the dissimilarity of trends along different directions, first, the gap of the $\Gamma \rightarrow K$ transition makes the Janus structure an indirect semiconductor for strain values higher than -1.8%. Second, the $\Gamma \rightarrow M$ transition influences the gap of the Janus structure and sustains the indirect semiconductor character with different electronic characteristics. In addition, the splitting due to the spin-orbit interaction that occurred at the K symmetry point is stronger than the splitting that occurred at the M symmetry point.

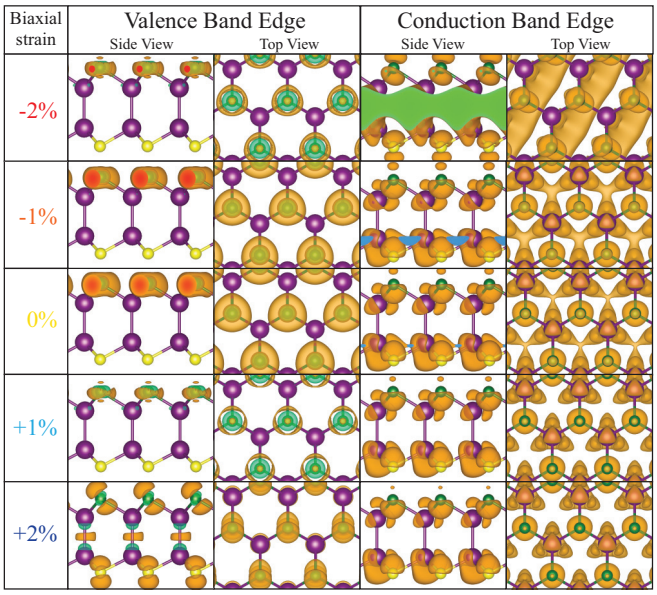

FIG. 4. Band-decomposed charge densities (side view and top view) of the valence-band edge and conduction-band edge of the Janus In_2SSe single layer under biaxial strain. The isosurface level was taken to be 1.15×10^{-5} electrons/Å^3.

Therefore, transitions between $\Gamma \rightarrow M$ and $\Gamma \rightarrow K$ indicate varieties in the electronic property of the Janus structure.

Figure 4 shows band-decomposed charge densities of the Janus In_2SSe single layer at the valence-band edge and the conduction-band edge under biaxial strain. At a $+2\%$ strain value and a -2% strain value, the valence-band edge and conduction-band edge reside at the M point and the K-Γ point, respectively. Apart from these points, the Γ symmetry point determines the valence-band edge and conduction-band edge for other strain values. It can be seen that when the VBM point resides at Γ, Se atoms are dominant in electron charge density, which means the selenide side determines the VBM point in the Janus structure. Planar p_x and p_y orbitals are effective in the valence-band edge from -2% to $+1\%$ strain values. At a $+2\%$ strain value, the VBM point has a contribution from all atoms, especially from p_z orbitals of chalcogenide atoms. On the contrary, the sulfide side determines the CBM point dominantly in the In_2SSe single layer's electronic band diagram. Between -1% and $+2\%$ strain values, electrons flow through triangular regions that are formed by In atoms of sulfide side. Similarly, In atoms on the sulfide side guide electrons to travel in the zigzag direction at a -2% strain value. Additionally, since the CBM point resides at the Γ point, it can be seen that electrons in the Janus In_2SSe single layer behave as free electrons, and the conduction-band edge of the Γ point forms an extended state which is almost independent of strain.

V. CONCLUSIONS

In conclusion, we investigated a stable Janus single-layer structure, In_2SSe, via first-principles calculations. We showed that there is a strong relation between the structural and electronic properties of both ternary In_2SSe and binary analogs of the Janus single layer, InS and InSe. The dynamically stable

Janus structure protects the structural symmetry and geometry of its binary analogs and has a higher cohesive energy than the InSe single layer. For that reason, it was found that it is possible to achieve a Janus structure with sulfurization of the InSe single layer in proper experimental conditions. Additionally, it was noted that the electronic band structure of the ternary Janus structure is formed by the superposition of the strained electronic band structures of the binary analog single layers. Due to the meeting of the two counterstrained Janus halves, the Janus structure presents a direct band gap, in contrast to InS and InSe single layers, which are indirect band gap semiconductors. In addition, the strain-dependent electronic properties of the Janus In_2SSe single layer were also investigated. It was revealed that the Janus single layer exhibits robust direct band gap semiconductor behavior under tolerable strain. Therefore, the ternary Janus In_2SSe single layer is a good candidate for optoelectronic nanomaterials and nanodevices.

ACKNOWLEDGMENTS

Computational resources were provided by TUBITAK ULAKBIM, High Performance and Grid Computing Center (TR-Grid e-Infrastructure). H.S. acknowledges financial support from TUBITAK under Project No. 117F095.

[1] K. S. Novoselov, A. K. Geim, S. V. Morozov, D. Jiang, Y. Zhang, S. V. Dubonos, I. V. Grigorieva, and A. A. Firsov, Science **306**, 666 (2004).
[2] A. K. Geim and K. S. Novoselov, Nat. Mater. **6**, 183 (2007).
[3] R. A. Gordon, D. Yang, E. D. Crozier, D. T. Jiang, and R. F. Frindt, Phys. Rev. B **65**, 125407 (2002).
[4] K. F. Mak, C. Lee, J. Hone, J. Shan, and T. F. Heinz, Phys. Rev. Lett. **105**, 136805 (2010).
[5] J. N. Coleman, M. Lotya, A. O'Neill, S. D. Bergin, P. J. King, U. Khan, K. Young, A. Gaucher, S. De, R. J. Smith, I. V. Shvets, S. K. Arora, G. Stanton, H.-Y. Kim, K. Lee, G. T. Kim, G. S. Duesberg, T. Hallam, J. J. Boland, J. J. Wang, J. F. Donegan, J. C. Grunlan, G. Moriarty, A. Shmeliov, R. J. Nicholls, J. M. Perking, E. M. Grieveson, K. Theuwissen, D. W. McComb, P. D. Nellist, and V. Nicolosi, Science **331**, 568 (2011).
[6] Q. H. Wang, K. Kalantar-Zadeh, A. Kis, J. N. Coleman, and M. S. Strano, Nat. Nanotechnol. **7**, 699 (2012).
[7] H. Sahin, S. Tongay, S. Horzum, W. Fan, J. Zhou, J. Li, J. Wu, and F. M. Peeters, Phys. Rev. B **87**, 165409 (2013).
[8] J. S. Ross, P. Klement, A. M. Jones, N. J. Ghimire, J. Yan, D. G. Mandrus, T. Taniguchi, K. Watanabe, K. Kitamura, W. Yao, D. H. Cobden, and X. Xu, Nat. Nanotechnol. **9**, 268 (2014).
[9] B. Chen, H. Sahin, A. Suslu, L. Ding, M. I. Bertoni, F. M. Peeters, and S. Tongay, ACS Nano **9**, 5326 (2015).
[10] S. Cahangirov, M. Topsakal, E. Aktürk, H. Sahin, and S. Ciraci, Phys. Rev. Lett. **102**, 236804 (2009).
[11] M. E. Davila, L. Xian, S. Cahangirov, A. Rubio, and G. L. Lay, New J. Phys. **16**, 095002 (2014).
[12] P. Miro, M. Audiffred, and T. Heine, Chem. Soc. Rev. **43**, 6537 (2014).
[13] H. Sahin, E. Torun, C. Bacaksiz, S. Horzum, J. Kang, R. T. Senger, and F. M. Peeters, Wiley Interdiscip. Rev. Comput. Mol. Sci. **6**, 351 (2016).
[14] A. Gupta, T. Sakthivel, and S. Seal, Prog. Mater. Sci. **73**, 44 (2015).
[15] M. Naguib, V. N. Mochalin, M. W. Barsoum, and Y. Gogotsi, Adv. Mater. **26**, 992 (2014).
[16] B. Anasori, M. R. Lukatskaya, and Y. Gogotsi, Nat. Rev. Mater. **2**, 16098 (2017).
[17] J. Dai, M. Li, and X. C. Zeng, Wiley Interdiscip. Rev. Comput. Mol. Sci. **6**, 211 (2016).
[18] J. O. Island, A. J. Molina-Mendoza, M. Barawi, R. Biele, E. Flores, J. M. Clamagirand, J. R. Ares, C. Sanchez, H. S. J. van der Zant, R. D'Agosta, I. J. Ferrer, and A. Castellanos-Gomez, 2D Mater. **4**, 022003 (2017).
[19] R. W. Dawon and R. W. Redington, Phys. Rev. **96**, 1498 (1954).
[20] Z. Yang, W. Jie, C. H. Mak, S. Lin, H. Lin, X. Yang, F. Yan, S. P. Lau, and J. Hao, ACS Nano **11**, 4225 (2017).
[21] S. Lei, L. Ge, S. Najmaei, A. George, R. Kappera, J. Lou, M. Chhowalla, H. Yamaguchi, G. Gupta, R. Vajtai, A. D. Mohite, and P. M. Ajayan, ACS Nano **8**, 1263 (2014).
[22] G. W. Mudd, S. A. Svatek, T. Ren, A. Patane, O. Makarovsky, L. Eaves, P. H. Beton, Z. D. Kovalyuk, G. V. Lashkarev, Z. R. Kudrynskyi, and A. I. Dmitriev, Adv. Mater. **25**, 5714 (2013).
[23] G. W. Mudd, M. R. Molas, X. Chen, V. Zolyomi, K. Nogajewski, Z. R. Kudrynskyi, Z. D. Kovalyuk, G. Yusa, O. Makarovsky, L. Eaves, M. Potemski, V. I. Fal'ko, and A. Patane, Sci. Rep. **6**, 39619 (2016).
[24] D. A. Bandurin, A. V. Tyurnina, G. L. Yu, A. Mishchenko, V. Zolyomi, S. V. Morozov, R. K. Kumar, R. V. Gorbachev, Z. R. Kudrynskyi, S. Pezzini, Z. D. Kovalyuk, U. Zeitler, K. S. Novoselov, A. Patane, L. Eaves, I. V. Grigorieva, V. I. Fal'ko, A. K. Geim, and Y. Cao, Nat. Nanotechnol. **12**, 223 (2016).
[25] A. S. Nissimagoudar, J. Ma, Y. Chen, Wu Li, J. Phys.: Condens. Matter **29**, 335702 (2017).
[26] M. Brotons-Gisbert, D. Andres-Penares, J. P. Martinez-Pastor, A. Cros, and J. F. Sanchez-Royo, Nanotechnology **28**, 115706 (2017).
[27] T. Nishino and Y. Hamakawa, Jpn. J. Appl. Phys. **16**, 1291 (1977).
[28] V. Zolyomi, N. D. Drummond, and V. I. Fal'ko, Phys. Rev. B **89**, 205416 (2014).
[29] Y. C. Cheng, Z. Y. Zhu, M. Tahir, and U. Schwingenschlögl, Europhys. Lett. **102**, 57001 (2013).
[30] Q.-F. Yao, J. Cai, W.-Y. Tong, S.-J. Gong, J.-Q. Wang, X. Wan, C.-G. Duan, J. H. Chu, Phys. Rev. B **95**, 165401 (2017).
[31] A.-Y. Lu, H. Zhu, J. Xiao, C.-P. Chuu, Y. Han, M.-H. Chiu, C.-C. Cheng, C.-W. Yang, K.-H. Wei, Y. Yang, Y. Wang, D. Sokaras, D. Nordlund, P. Yang, D. A. Muller, M-Y. Chou, X. Zhang, and L.-J. Li, Nat. Nanotechnol. **12**, 744 (2017).
[32] J. Zhang, S. Jia, I. Kholmanov, L. Dong, D. Er, W. Chen, H. Guo, Z. Jin, V. B. Shenoy, L. Shi, and J. Lou, ACS Nano **11**, 8192 (2017).

[33] G. Kresse and J. Hafner, Phys. Rev. B **47**, 558 (1993).
[34] G. Kresse and J. Furthmuller, Phys. Rev. B **54**, 11169 (1996).
[35] J. P. Perdew, K. Burke, and M. Ernzerhof, Phys. Rev. Lett. **77**, 3865 (1996).
[36] S. Grimme, J. Comput. Chem. **27**, 1787 (2006).
[37] J. Heyd, G. E. Scuseria, and M. Ernzerhof, J. Chem. Phys. **118**, 8207 (2003).
[38] G. Henkelman, A. Arnaldsson, and H. Jonsson, Comput. Mater. Sci. **36**, 354 (2006).
[39] A. Togo, F. Oba, and I. Tanaka, Phys. Rev. B **78**, 134106 (2008).